Electrostatics of metallic surfaces in periodic density functional theory simulations within and beyond the linear response regime

Ivan Scivetti [1,*] Nikitas I. Gidopoulos [2] and Gilberto Teobaldi [3]

[1]*Scientific Computing Department, STFC UKRI, Daresbury Laboratory, Warrington WA4 4FS, United Kingdom*
[2]*Department of Physics, Durham University, South Road, Durham DH1 3LE, United Kingdom*
[3]*Scientific Computing Department, STFC UKRI, Rutherford Appleton Laboratory, Harwell Campus, Didcot OX11 0QX, United Kingdom*

It has been more than fifty years already since the first ever density functional theory (DFT) simulation of a jellium surface demonstrated that uniform electric fields and external point charges induce equivalent electrostatics in the limit of linear response. During the years that followed, improved jellium models and computational resources allowed including strong electric fields to explore the problem beyond linear response. Nowadays, most DFT simulations of metallic surfaces are routinely conducted using finite slabs with periodic boundary conditions (PBCs) and the pseudopotential method to account explicitly for the ionic lattice. Surprisingly, there is apparently no record of dedicated studies that jointly discuss how the electrostatic response of metallic slabs in strong electric fields is affected by the PBCs, the net charge, the number of atomic layers, the surface orientation, and the adopted exchange-correlation potential. To investigate these points, we carry out detailed DFT simulations for the low-index facets of Li, Al, and Ag of neutral and charged slabs for varying ranges of external fields. Using key response parameters, we quantify and compare the electrostatics of slabs within and beyond the linear response regime and find that neutral and charged slabs exhibit equivalent responses for equivalent external perturbations. This analysis also offers a numerical demonstration that the electrostatic equivalence for the original jellium model also applies to slabs of finite size in PBCs. Our findings do not only invite the revision of some standard approximations to characterize the electrostatic response of metallic slabs but also aim to support the development of semiclassical, DFT-based methods for metallic interfaces using PBCs.

I. INTRODUCTION

Over five decades ago, N. D. Lang and W. Kohn applied the Kohn-Sham (KS) formulation [1] of density functional theory (DFT) [2] for the very first time to compute the quantum problem of metallic surfaces using the jellium approximation [3–5]. This seminal contribution revolutionized the field of surface science and made of computational simulations an invaluable tool to support experiments since then [6].

One of the most important contributions of N. D. Lang and W. Kohn (LK) was the demonstration that weak uniform electric fields and external point charges induce equivalent electrostatic responses of the jellium surface [5]. This equivalence (LK equivalence hereinafter) was demonstrated to be valid only in the linear response regime for jellium surfaces of infinite area. Nowadays, most of the available DFT codes allow computing systems of finite size in periodic boundary conditions (PBCs) adopting the pseudopotential (PP) method to account for the ionic lattice [7,8]. Surfaces are routinely

modelled using slabs composed of few atomic layers with the surface orientation of interest, while a vacuum region is included to minimize the spurious electrostatic interaction from the infinite replicas.

To our knowledge, the LK equivalence has not been yet demonstrated for metallic slabs in PBCs. Surprisingly, we neither found reported studies that exclusively analyze how the electrostatic response of vacuum-exposed metallic slabs in PBCs is affected by the net charge state, the number of atomic layers, the surface orientation, and the adopted exchange-correlation (XC) potential. We believe that over the years researchers must have accounted for some of these variables via convergence tests applied to specific problems [9–12]. Nevertheless, there is no evidence of a dedicated study addressing all these points jointly. As discussed later in the text, such an overlooked gap constrains the development of semiclassical, DFT based methods for charge transfer only to metallic surface models of sufficiently large areas, which is the linear response limit of the LK equivalence. As most of the available DFT codes for computational surface science use PBCs, it is then relevant to investigate the electrostatics of finite slabs beyond the linear response.

In this work, we have carried out detailed DFT simulations for the low-index facets of Li, Al, and Ag using neutral and charged slabs under strong external fields. The choice of Li, Al, and Ag is made to account for examples of alkali, p-block, and noble metals, respectively. Based on previous work, we

*ivan.scivetti@stfc.ac.uk

have computed key parameters that allows quantifying the electrostatics beyond linear response. From interpolation of such computed parameters, we can also access the limit of linear response and explore the validity of the LK equivalence for finite slabs.

It is worth to briefly summarize the long but thrilling history of DFT applied to metallic surfaces, particularly when exposed to external fields.[1] Following the work of LK [3–5], the improvement of computational resources in the eighties led to the first self-consistent DFT simulations of jellium beyond linear response, which provided unprecedented information of the differential capacity at interfaces as well as details of optical properties [16–21]. The first DFT simulations including PPs explicitly were conducted by solving the one-dimensional problem in a surface-averaged effective potentials [22–24], which made it possible to estimate the image plane position and its dependence on the crystallographic orientation. With the incorporation of PPs over the full 3D-space, the use of finite slabs in PBCs enabled the first DFT simulations of surfaces with unprecedented detail of the electronic structure. Simulations have considered the interaction with either external point charges [9,10], charged sheets [11,12] and uniform electric fields [25–27]. Since the late nineties, a large amount of DFT studies have followed to address diverse problems such as field evaporation [28], second-harmonic generation [29], surface reconstruction [30,31], stress to excess charge [32], and metal/solvent interfaces [33]. The list of reported DFT studies is endless.

The main reason motivating the present work is that, despite its success, practical DFT still has severe limitations to reproduce many relevant surface effects (see below). This is mainly due to the incapability of local XC functionals to properly describe the interactions at the surface region, where the electron density exhibits a near-discontinuity and the highly nonlocal electronic correlations cannot be captured by local approximations [34,35]. Part of these limitations has been overcome by the development of vdW-corrected XC functionals, which significantly improved the description of physical phenomena at interfaces [36,37]. Even so, standard semilocal DFT fails to reproduce the correct asymptotic behavior of the potential into the vacuum region, thus precluding the correct description of electron tunneling [38] and image states [39,40]. Recent developments in meta-GGA XC approximations [41] have however shown great promise in improving the asymptotic behavior. Although constrained-DFT solutions [42–44] allows tackling the problem of fractional charging, there is no yet a well-established methodology that can efficiently compute hybridization at metallic interfaces, for which charge transfer applications have been restricted to the weak coupling regime where atoms or molecules are not bound to the surface [43].

In principle, most DFT limitations can be remedied through many-body perturbation theory [40,45], but the

implementations of such solutions to the problem of metallic slabs including electrostatic perturbations are not yet available. Within this framework, we believe that further development of semiclassical, DFT-based methods can offer a good strategy to circumvent some of the inherent limitations of DFT for metallic surfaces. One of these semiclassical method is DFT-PC, developed by one of us to compute molecular adsorbates on insulating films supported by metallic substrates [46–49]. In this scheme, the whole metal substrate is replaced by a perfect conductor (PC), and the DFT problem of adsorbate and film is computed self-consistently in the potential generated by the induced charge at the PC.

As for any semiclassical method, the use of classical charge distributions like the PC to approximate the electrostatic response of the metallic surface requires a deep understanding of how the explicit metallic slab responds to external perturbations. In fact, for a metallic slab of finite area A in PBCs, the transfer of charge Q_s to a separated species will induce a non-zero-average surface charge density $-Q_s/A$ at the slab surface. The generated electrostatic response at the slab will differ from the response generated if the charge density was Q_s/A. Comparing such responses is relevant to the present work, which can potentially contribute to, for example, the computation of image-charge effects in single-molecule junctions [50,51] as well as analytical models for metal/graphene interfaces [52]. Thus we consider that revising the DFT computation of metallic slabs in external fields is timely and relevant to current and future DFT-based research at interfaces.

The paper is organized as follows. Section II discusses the theoretical aspects of this work. Computational details are given in Sec. III. The electrostatic response for neutral slabs in external fields (Sec. IV) and net charged slabs interacting with a PC plane (Sec. V) are compared in Sec. VI. The role of the XC is investigated in Sec. VII. Finally, we discuss the conclusions in Sec. VIII. We also provide a extensive supporting information [53] not only with results that complement our research but also with a brief self-contained DFT formulation applied to this study for the interested reader.

II. THEORETICAL FRAMEWORK

In this work, we shall only focus on the electrostatic response of metallic surfaces under static electric fields. The type of electric fields considered are those generated by an uniform surface charge distribution, σ_{ext}, located in the vacuum region sufficiently far from outermost atomic layers of the metallic slab. Frequency dependent response and the well-know limitation of standard local exchange-correlation functionals are not considered in the present study. This restriction excludes cases such as the computation of images states [34,39,40,54–61] and the long-standing problem of a single electron interacting with a metallic surface [5,9,10,62–65].

Here we shall use the supercell approximation with PBCs and consider slab models with surface area A parallel to the xy plane and perpendicular to the z direction with $z \in [0, L_z]$, where the $z = 0$ and L_z are equivalent via the PBCs. The supercell also includes a sufficiently large vacuum region to minimize the interactions the periodically repeated slabs. The

---

[1]In parallel to DFT studies, the response of metallic surfaces under strong external fields has also been investigated using surface-embedded Green function formalism, developed by J. E. Inglesfield and collaborators [13–15].

DFT formulation for slabs with PBCs is well known. Even so, for the sake of completeness and for those interested readers who are not familiar with the mathematical foundations, we provide the basics of the DFT formulation for metallic slabs in Sec. I of Ref. [53].

To investigate the electrostatic response of metallic surfaces, we will use (i) neutral slabs under electric fields (Sec. II A) and (ii) the DFT-PC formalism [46], where the simulated slab can exchange charge with a perfect conductor (PC) located in the vacuum region (Sec. II B). Based on previous work, we shall use key parameters derived from the induced surface charges to characterize the electrostatic response (Sec. II C). Although not considered in the present work, and mainly for reference purposes, we also describe two other possible DFT methods to compute metallic slabs beyond linear response.

A. Neutral slab in uniform electric field

Let us assume a neutral slab with a sufficiently large vacuum region. An uniform external electric field, $\mathbf{E} = E_z\hat{\mathbf{k}}$, is applied across the supercell, with $\hat{\mathbf{k}}$ the unit vector in the z direction. The mathematical foundations for the DFT problem of neutral slabs in uniform electric fields with PBCs were laid down over two decades ago [25,66]. The interested reader is referred to Sec. II of Ref. [53] for a brief description of the theory. It is important to reiterate that the DFT computation of neutral metallic slabs under (strong) fields using the PP approximation is not new [67]. Here, we use this methodology to compute the electrostatic response and compare results against the problem of charged slabs interacting with an external PC (see Sec. II B).

Since the electric field is screened inside the (neutral) metallic slab, the overall response is the accumulation of opposite charge at both sides of the slab. An example of such distribution will be discussed in Sec. IV. This charge distribution generates a net dipole moment in the system, which requires of a dipole potential to correct the electrostatics in PBCs. An efficient DFT solution to this problem was first proposed by J. Neugebauer and M. Scheffler [25] and later corrected by L. Bengtsson [66]. The accumulation of opposite charge at both surfaces indicates that the electrostatic response at each side of the slab can be seen as two complementary surface models within the same slab. Here, we refer to z_σ as the z-coordinate inside the slab that separates the positive and negative sides of the slab. In the region $0 \leqslant z < z_\sigma$ the vector normal to the surface $\hat{\mathbf{n}}$ is $-\hat{\mathbf{k}}$ and the normal component of the external field $E_{nz} = E_z(\hat{\mathbf{n}} \cdot \hat{\mathbf{k}}) = -E_z$. Consequently, we have $\hat{\mathbf{n}} = \hat{\mathbf{k}}$ in the region $z_\sigma < z < L_z$, and the normal component of the external field $E_{nz} = E_z(\hat{\mathbf{n}} \cdot \hat{\mathbf{k}}) = E_z$.

Following the DFT simulation of the slab in an external field $E_z\hat{\mathbf{k}}$, the computed electrostatic potential, $V_{el}(\mathbf{r}; E_z)$, and the corresponding self-consistent charge density, $\rho(\mathbf{r}; E_z)$, are represented in a grid within a supercell. The induced potential $\rho_{ind}(\mathbf{r}, E_z)$ for each side of the slab is defined as follows:

$$V_{ind}(\mathbf{r}; -E_z) = V_{el}(\mathbf{r}; E_z) - V_{el}^0(\mathbf{r}) \quad 0 \leqslant z < z_\sigma,$$
$$V_{ind}(\mathbf{r}; E_z) = V_{el}(\mathbf{r}; E_z) - V_{el}^0(\mathbf{r}) \quad z_\sigma \leqslant z < L_z. \quad (1)$$

where $V_{el}^0(\mathbf{r}) = V_{el}(\mathbf{r}; E_z = 0)$ is the potential in absence of an external electrical field. It is important to remark that both

induced potentials $V_{ind}(\mathbf{r}; E_z)$ and $V_{ind}(\mathbf{r}; -E_z)$ are derived from the same common $V_{el}(\mathbf{r}; E_z)$ but interpreted to be the result of exposing either side of the slab to external fields of different signs. Analogously, we define the induced charge density $\rho_{ind}(\mathbf{r}, E_z)$ with the following expression:

$$\rho_{ind}(\mathbf{r}; -E_z) = \rho_{el}(\mathbf{r}; E_z) - \rho_{el}^0(\mathbf{r}) \quad 0 \leqslant z < z_\sigma,$$
$$\rho_{ind}(\mathbf{r}; E_z) = \rho_{el}(\mathbf{r}; E_z) - \rho_{el}^0(\mathbf{r}) \quad z_\sigma \leqslant z < L_z, \quad (2)$$

with $\rho^0(\mathbf{r}) = \rho(\mathbf{r}; E_z = 0)$ being the charge density in absence of an external field (unperturbed slab).

For the purpose of analysis and visualization, it is common practice to define the xy-averaged induced potential

$$\phi_{ind}(z; \pm E_z) = \frac{1}{A} \int_A V_{ind}(\mathbf{R}, z; \pm E_z) d\mathbf{R} \quad (3)$$

and the xy-averaged induced surface density

$$\sigma_{ind}(z; \pm E_z) = \frac{1}{A} \int_A \rho_{ind}(\mathbf{R}, z; \pm E_z) d\mathbf{R} \quad (4)$$

at each side of the slab. The external electric field $\mathbf{E} = E_z\hat{\mathbf{k}}$ can be rationalized as the field in between two uniformly charged sheets located at the boundaries of the supercell. From elementary electrostatics we find $E_z = -4\pi\sigma_{ext}$, where σ_{ext} is the surface charge density at one of the capacitors ($-\sigma_{ext}$ at the other capacitor) [68]. Let us place one of these external sheets with charge density σ_{ext} at $z = 0$, and the other external sheet with charge density $-\sigma_{ext}$ at $z = L_z$.[2] The slab in the region $0 \leqslant z < z_\sigma$ is exposed to a field $-2\pi\sigma_{ext} = E_z/2$ generated by σ_{ext} at $z = 0$. Thus the total induced surface charge σ_{ind}^* is defined as

$$\sigma_{ind}^*(-E_z) = \int_0^{z_\sigma} \sigma_{ind}(z; -E_z) dz = -\sigma_{ext}\bigg|_{z=0} \quad (5)$$

and will generate an electric field E_z between the sheet at $z = 0$ and the first atomic layer (sufficiently far from this layer). Similarly, the slab in the region $z_\sigma \leqslant z < L_z$ is exposed to a field $2\pi\sigma_{ext}$ generated by $-\sigma_{ext}$ at $z = L_z$, and this induces a total charge density per unit area σ_{ind}^*. Thus

$$\sigma_{ind}^*(E_z) = \int_{z_\sigma}^{L_z} \sigma_{ind}(z; E_z) dz = \sigma_{ext}\bigg|_{z=L}. \quad (6)$$

Since the slab is neutral we have

$$\int_0^{z_\sigma} \sigma_{ind}(z; -E_z) dz = -\int_{z_\sigma}^{L_z} \sigma_{ind}(z; E_z) dz. \quad (7)$$

Either Eq. (5) or (6) can be used to obtain z_σ within the slab. In the linear response limit, z_σ will be at the center of the slab, but this is not necessarily true beyond the linear response. We will return to this point in Sec. IV.

B. The DFT-PC method

The DFT-PC method is a DFT-based approach that allows computing a charged system (here a charged slab) interacting

---

[2]Numerically, the location of the charged sheets are set at Δz and $L_z - \Delta z$, as few grid points are needed to correct for PBCs along the z direction.

with an external perfect conductor PC located at z_{pc} in the vacuum region [46]. In Sec. III A of Ref. [53] we provide a mathematical description of the DFT-PC method for the interested reader. The method allows setting a net amount of charge for the slab to Q_s, which automatically fixes a total charge of $-Q_s$ at the PC plane, thus maintaining the neutrality of the supercell. Here, the charge density at the PC is set to be uniformly distributed in the xy plane, i.e., $\sigma_{pc}(\mathbf{r}) = -Q_s/A\delta(z - z_{pc})$. The choice of this functional form for $\sigma_{pc}(\mathbf{r})$ does not correspond to the charge distribution of a point charge Q_s required to test the KL equivalence. However, due to PBCs in the xy plane, $\sigma_{pc}(\mathbf{r})$ is a good approximation to the point charge distribution for sufficiently large separation from the slab (see Sec. III B of Ref. [53]).

The surface charge density $\sigma_{pc}(\mathbf{r})$ generates an electrostatic potential that is included self-consistently in the DFT computation of the charged slab. This leads to the accumulation of opposite charge only at the side of the slab closest to the PC plane. Due to the PBCs, the z position of the plane for dipole corrections must be set in the vacuum region between the PC plane an the opposite side of the slab [46].

Following the DFT-PC computation of the slab with net charge Q_s, we obtain the electrostatic potential $V_{el}(\mathbf{r}; \sigma_{pc}^*)$ and the charge density, $\rho(\mathbf{r}; \sigma_{pc}^*)$, where $\sigma_{pc}^* = \int_{\mathcal{V}} \sigma_{pc}(\mathbf{r}) d\mathbf{r} = -Q_s/A$ is the total charge per unit area at the PC plane. Similarly to Eqs. (1) and (2), we define the induced potential, $V_{ind}(\mathbf{r}; \sigma_{pc}^*)$, as follows:

$$V_{ind}(\mathbf{r}; \sigma_{pc}^*) = V_{el}(\mathbf{r}; \sigma_{pc}^*) - V_{el}^0(\mathbf{r}), \qquad (8)$$

where $V_{el}^0(\mathbf{r}) = V_{el}(\mathbf{r}; \sigma_{pc}^* = 0)$ is the potential for the neutral system. Note that $V_{el}(\mathbf{r}; \sigma_{pc}^* = 0) = V_{el}(\mathbf{r}; E_z = 0)$. The induced charge density, $\rho_{ind}(\mathbf{r}; \sigma_{pc}^*)$, is the charge response from the interaction with the PC and

$$\rho_{ind}(\mathbf{r}; \sigma_{pc}^*) = \rho(\mathbf{r}; \sigma_{pc}^*) - \rho^0(\mathbf{r}) \qquad (9)$$

with $\rho^0(\mathbf{r}) = \rho(\mathbf{r}, \sigma_{pc}^* = 0)$. Note that $\rho(\mathbf{r}; \sigma_{pc}^* = 0) = \rho(\mathbf{r}; E_z = 0)$ is the computed charge density of the unperturbed slab. Similarly to Eqs. (3) and (4), we define the xy-averaged induced potential $\phi_{ind}(z; \sigma_{pc}^*)$ as

$$\phi_{ind}(z; \sigma_{pc}^*) = \frac{1}{A} \int_A V_{ind}(\mathbf{R}, z; \sigma_{pc}^*) d\mathbf{R}, \qquad (10)$$

and the xy-averaged induced surface charge, $\sigma_{ind}(z; \sigma_{pc}^*)$, with the following expression:

$$\sigma_{ind}(z; \sigma_{pc}^*) = \frac{1}{A} \int_A \rho_{ind}(\mathbf{R}, z; \sigma_{pc}^*) d\mathbf{R}. \qquad (11)$$

C. Parametrizing the electrostatic response

Since the work of LK [3–5], computed profiles for σ_{ind} have been used to characterize and parametrize the electrostatic response of metallic surfaces. One of these parameters is the centroid of the induced charge distribution, z_c. Following the formulas of Sec. II A for a neutral slab in an external field $\mathbf{E} = E_z \hat{\mathbf{k}}$, we have

$$z_c(E_{nz} = -E_z) = \frac{\int_0^{z_\sigma} z \sigma_{ind}(z; -E_z) dz}{\int_0^{z_\sigma} \sigma_{ind}(z; -E_z) dz} \qquad (12)$$

and

$$z_c(E_{nz} = E_z) = \frac{\int_{z_\sigma}^{L_z} z \sigma_{ind}(z; E_z) dz}{\int_{z_\sigma}^{L_z} \sigma_{ind}(z; E_z) dz} \qquad (13)$$

at each side of the slab, where E_{zn} is the component of the external field $\mathbf{E}$ normal to the surface. For a charged slab interacting with an external PC, the integration is over the whole z domain and we have

$$z_c(\sigma_{pc}^*) = \frac{\int_0^{L_z} z \sigma_{ind}(z; \sigma_{pc}^*) dz}{\int_0^{L_z} \sigma_{ind}(z; \sigma_{pc}^*) dz}. \qquad (14)$$

Another relevant parameter is obtained from the evidence that σ_{ind} reaches a maximum (or minimum) value outside the slab [see Figs. 1(c) and 2(d) below]. The full half width, λ, is defined as the extent for which σ_{ind} reaches half of this maximum (or minimum) value. λ is essentially a screening length and has been identified to play an important role for the optical response of the surface [17,69,70].

The computation of z_c and λ for $E_{nz} \to 0$ or $\sigma_{ind}^* \to 0$ is challenging due to numerical instabilities [3,67]. Here, we shall refer to these values as z_{c0} and λ_0, which is the limit of linear response. For neutral slabs, large numerical noise is often introduced as the magnitude of the external field is reduced. Similarly, for charged slabs we observe that the numerical noise increases as one reduces the amount of charge transferred to the PC. Due to these technical difficulties, z_{c0} and λ_0 are obtained via interpolation at $\sigma_{ind}^* = 0$ of the computed z_c and λ beyond linear response.

D. Alternative DFT strategies

In this section, we briefly describe two possible alternatives to compute the electrostatics of metallic slabs within the framework of the present work. Although these methods will not be applied to the present study, we will use results computed with these alternatives for comparison purposes.

The first strategy has been developed by S.C. Lam and R.J. Needs [12] and consists to adding a thin charged sheet at the center of the vacuum region, halfway in between the two surfaces of the periodically repeated slab models. Charge neutrality within the supercell is achieved via tuning the position of the Fermi level in the metal. This external charged sheet induces an external field, and the excess of charge (of opposite sign) added to the slab accumulates at both sides of the slab. This method is somehow similar to DFT-PC and has been successfully applied to investigate the screening of electric fields at aluminum surfaces [12], the rate-constant for an electron to tunnel from an inert gas atom into a metal surface [11], and the response of the surface stress to excess charge [32]. This method has also been extended using the grand-canonical DFT formalism [30] to simulate surface reconstruction of charged slabs at constant chemical potential [31] and investigate field evaporation phenomena [28]. Despite its success, the applicability of this method is restricted to slabs that are symmetric in the z direction for which the total dipole moment within the supercell is zero. In fact, by the time this method was first introduced, dipole corrections were not yet available in DFT codes.
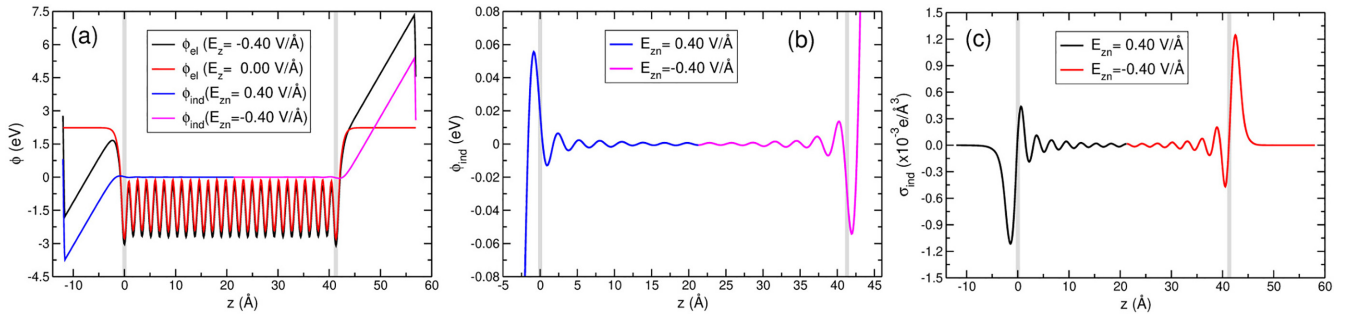
FIG. 1. Neutral slab model of Li(100) composed of 25 layers in a external electric field $\mathbf{E} = -0.40$ V/Å $\hat{\mathbf{k}}$. The z position of the outermost atomic layers of the slab are indicated by the grey vertical lines. The outermost layer at the left is set to $z = 0$Å. Dipole correction are set at $z = -12$Å. (a) Computed electrostatic potentials ϕ_{el} for $E_z = -0.40$ (black) and 0 V/Å (red). The induced potential at the left (right) side of the slab is shown in blue (magenta). Values for E_{zn} in the captions indicate the projection of $\mathbf{E}$ along the normal vector $\hat{\mathbf{n}}$ at each surface of the slab, $\hat{\mathbf{n}} = -\hat{\mathbf{k}}$ at the left and $\hat{\mathbf{n}} = \hat{\mathbf{k}}$ at the right. (b) Augmented display of ϕ_{ind}. (c) the computed induced surface charge σ_{ind} demonstrates that the metal slab screens the external field by electron and hole accumulation at the left and right sides of the slab, respectively.

The second option is constrained-DFT [42–44], in which the total energy functional is minimized by constraining the electronic charge to be localized in a pre-defined region of the space, offering a promising strategy to tackle the self-interaction error [35,71]. A. Souza *et al.* [43] have applied this method to compute the interface between a single benzene molecule and a slab of Li(100) with and without PBCs. By transferring charge between both fragments, they computed the electrostatic response of the Li(100) surface and extracted the energy level alignment. This method offers a robust DFT framework to explore the weak coupling regime. However, for rather small surface areas and/or large separation distances in PBCs, the method could predict unphysical states for electron transfer, as the charge would rather leak from the fragments driven by the electrostatic force if the constrains were removed. To address physically valid conditions in PBCs [72], it is needed to simulate slabs with large surface areas, which significantly increase the cost of the simulations.

III. COMPUTATIONAL DETAILS

All the calculations were carried out using the projector-augmented wave method [73] together with PBCs, as implemented in the VASP code [74–76]. Details for the computational implementation of the DFT-PC method within VASP are described in Ref. [46]. We have computed the low-index (100), (110), and (111) facets of Li, Al, and Ag slabs. For most of the simulations, the electronic exchange-correlation was treated according to the GGA-PW91 approximation [77]. For the Ag(111), we have also considered the LDA [78], PBE [79] and the nonlocal optB86B [36] exchange-correlation (XC) functionals.

We have used pseudopotentials (PPs) with one $(2s^2)$, three (s^2p^1), and eleven $(4d^{10} 5s^1)$ valence electrons for the Li, Al and Ag atoms, respectively. To converge the metallic states we have used the second order method of Methfessel-Paxton [80] with a smearing of 0.2 eV. In addition, we set tight energy convergence thresholds, always lower than 10^{-7} eV. This last requirement is crucial to properly converge the charge density, which significantly affects the computation of z_c.

We first computed the three elements in bulk. Details for these calculations and computed lattice parameters can be found in Table I of Ref. [53]. For Li and Al, we find it sufficient to set an energy cutoff of 400 eV and a k-point sampling of $11 \times 11 \times 11$ in the Monkhorst-Pack scheme. For Ag, we also computed the problem using a cutoff of 600 eV and a k-point sampling of $21 \times 21 \times 21$. For the LDA and PBE functionals, we find that results are practically independent of the k-point sampling and the energy cutoffs within the range of computed values. Computed lattice parameters are within 2.03% with respect to the experimental values.

Using the converged bulk structures, we built vacuum-exposed slab models for the (100), (110) and (111) facets. Adopted DFT settings and geometrical details are provided in the Table II of Ref. [53]. Li, Al, and Ag slabs are compared using the GGA-PW91 approximation with an energy cutoff of 400 eV. To compare the results of different XC functionals for the Ag(111) surface, we have increased the cutoff to 600 eV.

We find that increasing the cutoff for the GGA-PW91 has a negligible effect in the computed values of z_c and λ. This is because such response parameters are computed from electronic charge differences. We have explored several k-point samplings and verified convergence in the computed values. Thus we are confident that the parameters listed in the Table II of Ref. [53] are sufficient to the purpose of the present study.

To analyze the role of the slab thickness, we have only considered the three facets of Li, and computed models with different number of atomic layers, ranging from 4 to 25 layers (one atom per layer) for the (100) and (111) facets and from 4 to 18 layers (two atoms per layer) for the (110) facet.

As in previous work [12,31], we have not considered the ionic relaxation of the slabs. This is because we will report the computed values of z_c with respect to the jellium edge (see Sec. VIC), so that we can compare our results directly with previous data. If surface relaxation is allowed, the interlayer separation distances are not the same across the slab, and the position of the jellium edge is not well defined. The role of surface relaxation, and the ensuing need for averaging or smoothing approaches [81] to unambiguously define jellium edges in the presence of atomic surface roughness, particularly for strong external perturbations of positively charged slabs, is beyond the primary aim of the paper, namely, numerically confirming the KL equivalence for pseudopotential-based, periodic metallic slabs.
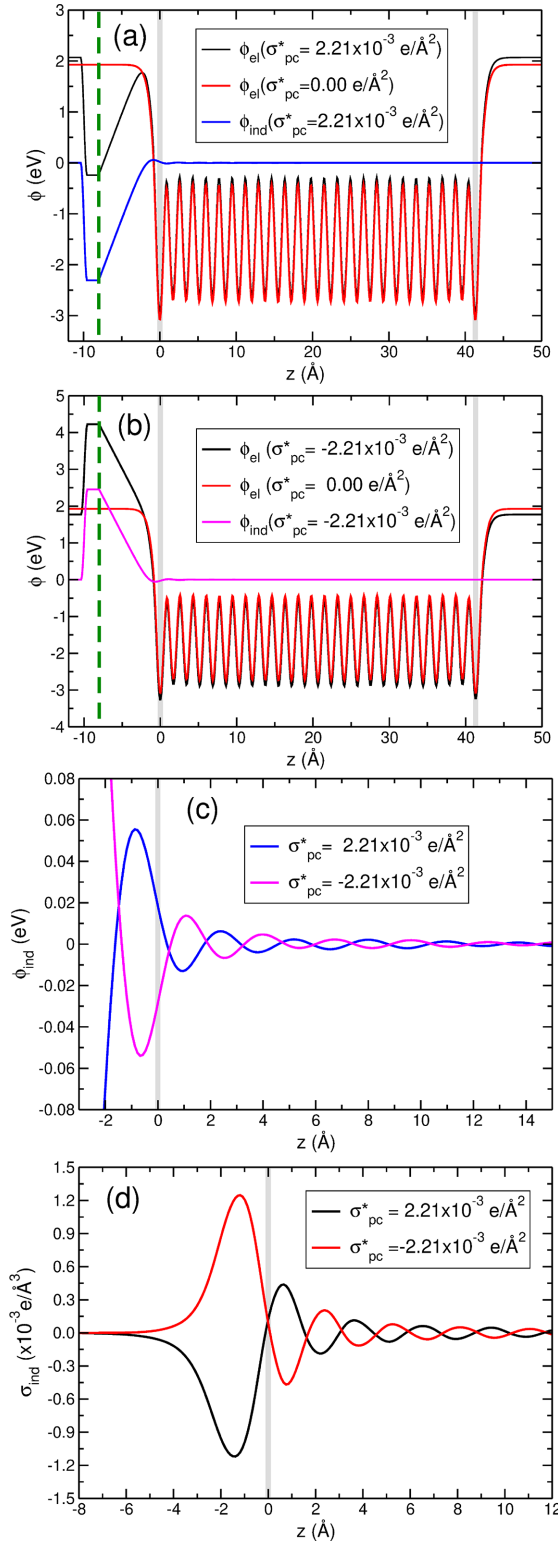
FIG. 2. Slab model for Li(100) surface (25 atomic layers) interacting with an external PC located $z = -8$Å (vertical green dashed line). The dipole correction is at $z = -10$Å. The z position of the outermost atomic layers of the slab are indicated by the grey vertical lines. (a) Computed electrostatic ϕ_{el} (black) and induced (blue) potentials for $\sigma^*_{pc} = 2.21 \times 10^{-3}$ e/Å^2. (b) Computed electrostatic ϕ_{el} (black) and induced (magenta) potentials for $\sigma^*_{pc} = -2.21 \times 10^{-3}$ e/Å^2. The electrostatic potential for the unperturbed slabs (red) is shown in (a) and (b). (c) Augmented display of the computed induced potentials. (d) Induced surface charge densities.

To compare the response of neutral and charged slabs using the two methods explained above, it is necessary to set equivalent external perturbations. To induce the same amount of surface charge density σ^*_{ind} at the relevant side of the slab (i) an external field of value $E_z = 4\pi \sigma^*_{ind}$ must be applied to the neutral slab and (ii) a total surface charge of $\sigma^*_{pc} = -\sigma^*_{ind}$ must be set at the PC plane, which will generate an external field E_z outside the slab. In Sec. VI C, the electrostatic responses are compared against the induced charge density σ^*_{ind}.

A crucial point is to set a sufficiently large vacuum region, which inevitably increases the computational cost for computations using plane waves. Nevertheless, large electric fields can lead to electron leakage from the slab to the vacuum region. This is a well-know phenomenon related to the process of electron field emission [72,82,83], extensively studied for many decades and beyond the scope of the present work [84,85]. To the purpose of the present study, we have based on the work of P. J. Fiebelman [72] and brought the position of the dipole layer (and the PC plane for the DFT-PC method) closer to the slab surface as the value of σ^*_{ind} become more negative. Likewise, we have also made sure to exclude those results where electron leakage was manifested. This is a tedious task but to date the only way forward to compute this type of problems using plane waves.

Finally, induced potentials are plotted such that the Fermi energy is set to zero inside the slab.

IV. NEUTRAL SLAB IN UNIFORM ELECTRIC FIELD

Figure 1 shows the computed induced potential and charge across the simulation cell for a slab model of Li(100) composed of 25 atomic layers in an electric field of $\mathbf{E} = -0.40$ V/Å $\hat{\mathbf{k}}$. As mentioned above, the problem is computed with the z coordinate defined between 0 and L_z (Sec. II A). However, to the purpose of visualization and analysis, we report the results by shifting the z values such that the outermost atomic layer at the left/bottom side of the slab is set to $z = 0$.

Such induced response is well known in the field [67]. We reiterate that the main purpose here is to briefly describe the computed quantities and compare results with those obtained using the DFT-PC method. In Fig. 1(a), we observe that the induced potential ϕ_{el} (solid black) exhibits a linear behavior at both sides of the slab, sufficiently far from the outermost atomic layers (grey vertical lines), and the dipole correction restores the periodicity at the edge of the slab. In absence of the electric field, the unperturbed slab is dipole-free and, consequently, the computed potential is flat in the vacuum region (solid red). The induced potential ϕ_{ind} at the left (right) side of the slab is shown in blue (magenta) and constitutes the net electrostatic response to the external field. Both profiles are augmented in Fig. 1(b), and show that the external field will tend to pull out (push in) electronic charge at the left (right) side of the slab, for which the normal component of the electric field, $E_{zn} = \mathbf{E} \cdot \hat{\mathbf{n}}$, is positive (negative). This leads to net electron and hole accumulations at the opposite sides of the slab, as shown in Fig. 1(c). Despite the finite size of the system, we observe an oscillatory pattern for σ_{ind} inside the slab, which is consistent with the Friedel oscillations observed for semi-infinite jellium surfaces [3–5,86]. The magnitude

of the oscillations for both ϕ_{ind} and σ_{ind} reduce towards the central part of the slab.

In semi-infinite models for metallic surfaces, the surface is an open system that can exchange electrons with a reservoir at constant chemical potential [25,46]. Here, nevertheless, the slab is a closed neutral system, and the electrostatic response is equivalent to transferring charge from one surface to the other. In other words, the whole electrostatic response can be seen as two complementary surface models that couple at z_σ inside the metal slab, where the condition of Eq. (7) is satisfied. If electron and hole distributions were equivalent, z_σ would be located at the middle of the slab. Nevertheless, from the calculation of z_σ for the three facets of Li using slab with different number of layers (Sec. VI B), we find that z_σ is always larger than 0.45 Å and smaller than 0.80 Å displaced from the geometrical center of the slab towards the positively charged side.

Finally, we have verified the importance of breaking the symmetry along the z direction, as explained in Sec. V of Ref. [53]. In fact, if the symmetry along the z direction is not broken, the computed charge density results to be symmetric with respect the center of the slab, leading to an incorrect potential that varies linearly even inside the metallic slab.

V. CHARGED SLAB INTERACTING WITH A PERFECT CONDUCTOR

Figure 2 shows the electrostatic response for the same slab model of the previous section, but in this case interacting with an external PC separated 8 Å from the outermost layer at the left, as indicated by the dashed green line. As for the results of previous section, we shifted the z values such that the outermost atomic layer at the left/bottom side of the slab is set to $z = 0$.

In contrast to the neutral slab subject to an external field where electron and hole accumulation are complementary responses, in this case, we need to compute the responses for electron and hole accumulation separately. Since we aim to compare the electrostatics of this system with the results of previous section, we must transfer charge from the slab to the PC such as the electric field between the PC and the slab is $E_z = 0.40$ and -0.40 V/Å (in two separate calculations). This is accomplished by setting a total surface charge σ_{pc}^* equal to 2.21 and -2.21×10^{-3} e/Å^2, which induces a total surface charge σ_{ind}^* of -2.21 and 2.21×10^{-3} e/Å^2 at the slab, respectively.

In Fig. 2(a), we plot the computed electrostatic potential ϕ_{el} for $\sigma_{\mathrm{pc}}^* = 2.21 \times 10^{-3}$ e/Å^2 (black). We notice that the potential is constant at the left of the PC, which demonstrates that the electrostatic potential is screened. In this particular case, the PC region is set to extend for 2 Å until $z_{\mathrm{dip}} = -10$Å where dipole corrections are applied. For this separation of 8.0 Å, we observe evidence of electron leakage for $\sigma_{\mathrm{pc}}^* > 2.76 \times 10^{-3}$ e/Å^2. Thus a density of $\sigma_{\mathrm{pc}}^* = 2.21 \times 10^{-3}$ e/Å^2 corresponds to a rather limiting scenario for the Li(100) model. Although the 2 Å separation between the PC and z_{dip} the could appear to be relatively small with respect to the extension of the slab, we have verified this does not affect the computed total energy. From the computation of the

unperturbed slab (red), we obtain the induced electrostatic potential (in blue).

In Fig. 2(b), we show results for $\sigma_{\mathrm{pc}}^* = -2.21 \times 10^{-3}$ e/Å^2. Since the slab is positively charged we do not have problem of electron leakage. Thus the PC region could in principle be extended to any value, but we have also kept it to 2 Å for the sake of comparison with the previous case. The induced electrostatic potential is shown in magenta. In Fig. 2(c), we augment the scale and compare the induced potentials in the same graph, where we observe an oscillatory patter that decreases towards the inner region of the metal slab. Computed induced charges σ_{ind} are displayed in Fig. 2(d), where we also observe a behavior consistent with the Friedel oscillations.

VI. ELECTROSTATIC RESPONSE OF NEUTRAL AND CHARGED SLABS

The two previous sections show how induced potentials and charges are computed using neutral slabs in external fields (method E_z) and charge slabs interacting with a PC (method PC). In this section, we compare the electrostatic response using both methods.

A. Induced potentials and charges

Figure 3 shows the induced potentials ϕ_{ind} [(a)–(c)] and induced surface charges σ_{ind} [(d)–(f)] for the (100) facet of Li, Al, and Ag. Results were computed using the GGA-PW91 XC potential. Details for the slab models are provided Table II of Ref. [53]. Empty squares refer to the method E_z (**E** = -0.40 V/Å $\hat{\mathbf{k}}$) and filled circles to the method PC ($\sigma_{\mathrm{pc}}^* = \pm 2.21 \times 10^{-3}$ e/Å^2). The same grid has been used for the computation of both methods. Results for hole accumulation at the right side of slabs computed with the method E_z [see Fig. 1 for the case of Li(100) facet] are projected to left side of the slab to allow comparison with the PC method. This explains the apparently different location for the z position of dots and squares.

From the plot, we find that both methods generate equivalent electrostatic responses. The same level of agreement between both methods is observed for the (110) and the (111) facets, as reported in Sec. IV of Ref. [53]. When comparing the profiles between the elements, we observe that the magnitude of the oscillations for ϕ_{ind} are larger for Li, followed by Ag and Al. For Al and Li, ϕ_{ind} exhibits oscillations that monotonically decay inside the slab, independently of the facet. For Ag, in contrast, smooth oscillations are only observed for the (110) facet, while for the other two facets the magnitude decay in a rather convoluted way. Consequently, computed σ_{ind} exhibit Friedel type oscillations for Li, Al, and Ag(110), while for Ag(100) and Ag(111) the excess charge is practically screened within 3 Å from the outermost atomic layer. Our results for Ag(111) are in qualitatively good agreement with the profile computed in Ref. [67].

Despite the observed agreement between both methods, comparing profiles for induced potentials and charges is useful only from a qualitative perspective. We could also plot differences but this also would be of little use. In addition, the agreement of Fig. 3 must be corroborated for a varying
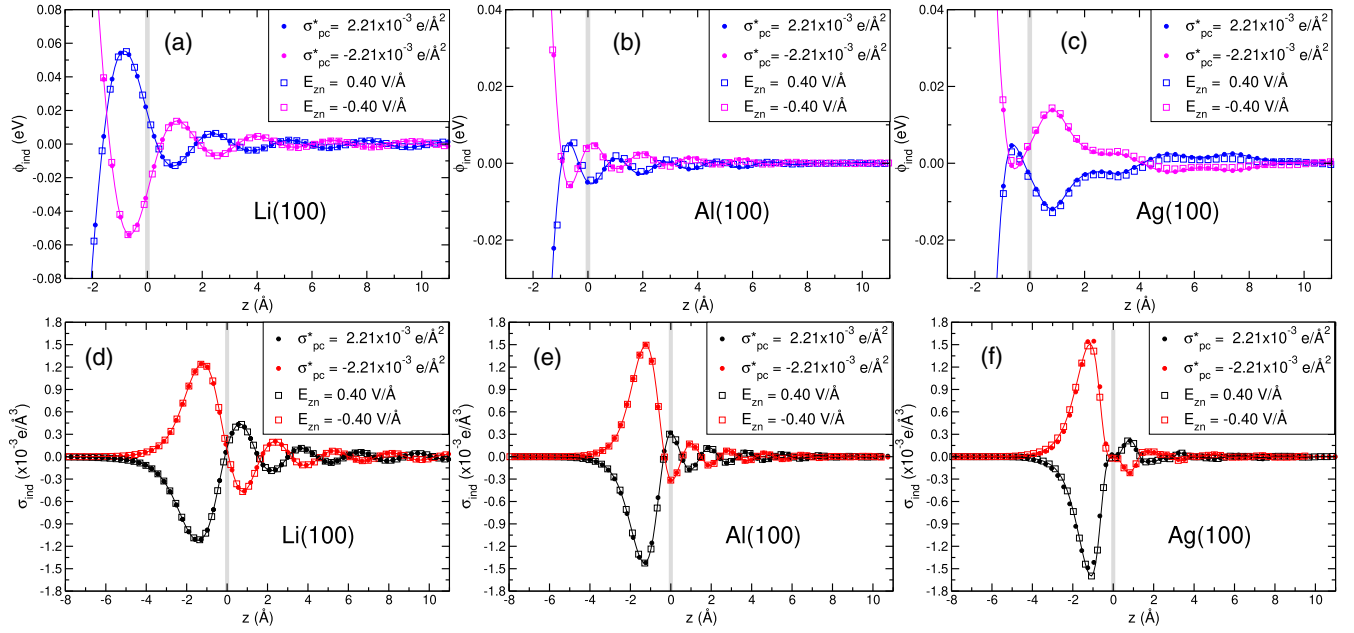
FIG. 3. Comparison of the induced potentials ϕ_{ind} [(a)–(c), blue and magenta] and surface charge densities σ_{ind} [(d)–(f), black and red] for Li, Al, and Ag in the (100) facet. Empty squares refer to the method E_z ($\mathbf{E} = -0.40$ V/Å $\hat{\mathbf{k}}$), and filled circles for the method PC ($\sigma_{pc}^* = \pm 2.21 \times 10^{-3}$ e/Å^2). Magenta and red describe hole accumulation, whereas blue and black electron accumulation. Solid lines are used as a guide to the eye.

range of external perturbations, which would further complicate the analysis. To facilitate identification of similarities and differences between the two methods, rather than comparing induced potentials and charges, we will focus on comparing z_c and λ, as defined in Sec. II C, to quantify the electrostatic response of slabs.

B. Dependence of the slab thickness

In this section, we evaluate the equivalence between the E_z and PC methods for Li slabs with different number of atomic layers. We shall keep the same external field $\mathbf{E} = -0.40$V/Å $\hat{\mathbf{k}}$ for neutral slabs (method E_z), and the same values total surface charge $\sigma_{pc}^* = \pm 2.21 \times 10^{-3}$e/Å^2 for the PC interacting with charged slabs (method PC).

Results for z_c are shown in Fig. 4 for induced electrons (a) and holes (b). Results for λ can be found in Fig. 3 of Ref. [53]. Despite small numerical uncertainties, we find a very good agreement between the computed values for neutral (empty squares, method E_z) and charged (filled circles, method PC) slabs. Thus, when using z_c as the parameter to quantify the electrostatic response of metallic surfaces, we can confidently claim within ± 0.1 Å (due to numerical errors) that the equivalence discussed in Sec. VI holds for slabs with a number of atomic layers larger $\geqslant 6$ for facets (100) and (111), and $\geqslant 4$ for the (110) surface. However, if instead of using condition of Eq. (7), we arbitrarily set z_σ at the half of the slab, we find that computed values for z_c do not converged with the number of atomic layers [see Fig. 4 of Ref. [53] for the Li(100) facet]. We find the dispersion for z_c is larger for electron accumulation, specially for the (111) facet, as the perturbation approach the limit of electron leakage. We also observe that z_c is different for electron and hole accumulation, which demonstrates that the accumulation of electrons and holes screen the external

perturbations differently, in agreement with previous research [16,17,67].

Finally, the trend for the z_c values remains practically constant with increasing the number of atomic layers of the modelled slabs, despite numerical uncertainties. The results demonstrate that each surface facet screens the external field differently. It is worth to emphasize that the present case of slabs in external fields differs from the standard problem of explicit adsorbates, deposited in metallic surfaces. For the latter, the adsorbate and the metallic surface form a bonded system, i.e., there is no external field, and the number of atomic layers needed to model the surface is routinely defined from the convergence of the adsorption energy.

C. Dependence on the perturbation strength

After having compared induced potentials and charges (Sec. VI) and analyzed the dependence of the response parameters with the number of layers for the modelled slabs (Sec. VI B), in this section, we evaluate the equivalence between the methods E_z and PC for different magnitudes of the external perturbation. To compare both methods, the settings must be such that they induce the same total induced charge per unit area, σ_{ind}^*, at the relevant side of the slab (see Sec. III). To facilitate the comparison of the computed z_c with previous work, we shall report the values with respect to z_J, which has been historically defined as the jellium edge, located at half the interlayer distance from the outermost atomic layer into the vacuum region.

Figures 5(a)–5(c) show $z_c - z_J$ for the low-index facets of Li, Al, and Ag as a function of σ_{ind}^* computed with the method PC. Values are always positive (outside the jellium edge), and increase as σ_{ind}^* decreases. However, the trend changes qualitative depending on the sign of σ_{ind}^*, particularly for Al
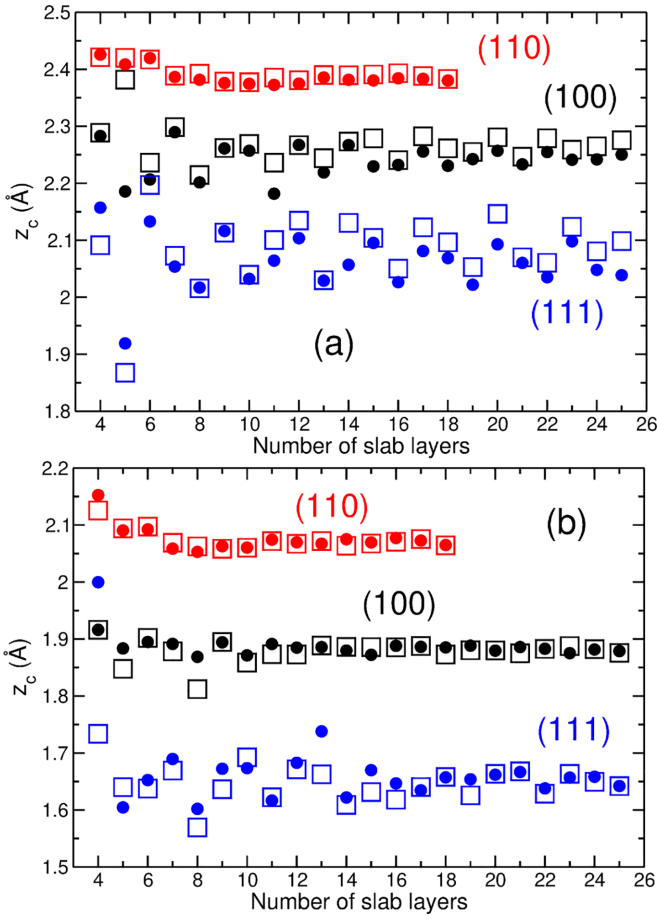
FIG. 4. Computed z_c for electron (a) and hole (b) accumulation as a function of the number of atomic layers for slab models of Li(100), Li(110) and Li(111), shown in black, red and blue, respectively. Empty squares correspond to values for neutral slabs in an external field of $E_{zn} = 0.40$ (a) and -0.40 V/Å (b). Filled circles correspond to charged slabs interacting with a PC with $\sigma_{pc}^* = 2.21 \times 10^{-3}$ e/Å^2 (a) and -2.21×10^{-3} e/Å^2 (b). Values are referred with respect to the outermost atomic layer.

and Ag: whereas values in the region $\sigma_{ind}^* > 0$ could be well adjusted with a linear fit, the behavior is qualitatively different for $\sigma_{ind}^* < 0$, where we notice a departure from linearity as σ_{ind}^* becomes less and less negative before electron leakage takes place. This trend is in agreement with previous findings for jellium [16,17]. It is important to reiterate that we have carefully checked there was not electron leakage in our results. The reduced domain for σ_{ind}^* when computing Li indicates that it is easier to induce electron leakage for this element in comparison to Al and Ag, which can be attributed to the lower work function (≈ 3.0 eV for Li in contrast to > 4.00 eV for Al and Ag). The solid lines are the result of fourth-order polynomial fitting to estimate the values of $z_c - z_J$ in the limiting case of $\sigma_{ind}^* = 0$ (see Table I below).

The computed differences Δz_c between the method PC and the method E_z are shown in Figs. 5(d)–5(f) for Li, Al and Ag. Nonzero values are observed for selected facets around $\sigma_{ind}^* = 0$. This is a consequence of unavoidable numerical errors when computing the integrals for small amounts of induced charge. Thus Δz_c for $|\sigma_{ind}^*| <$

TABLE I. Response parameters $z_{c0} - z_J$ and λ_0 in the limit of $\sigma_{ind}^* = 0$ computed with the method PC. Values are obtained from the interpolation of the computed data of Figs. 5 and 6. Values of columns $|\Delta z_{c0}|$ and $|\Delta\lambda_0|$ are the differences between method E_z and PC. Values are given in Å units.

Element	Facet	$z_{c0} - z_J$	$|\Delta z_{c0}|$	λ_0	$|\Delta\lambda_0|$
Li	(100)	1.166	0.002	1.999	0.004
	(110)	0.980	0.002	1.921	<0.001
	(111)	1.298	0.006	2.016	0.003
Al	(100)	0.648	0.001	1.478	0.005
	(110)	0.899	0.010	1.489	0.012
	(111)	0.566	0.010	1.476	0.003
Ag	(100)	0.504	0.005	1.319	0.017
	(110)	0.673	0.018	1.300	0.003
	(111)	0.409	<0.001	1.328	0.001

0.5×10^{-3}e/Å^2 should not be considered as a reference to compare the methods. Even so, $|\Delta z_c|$ is always lower than 0.04 Å for $\sigma_{ind}^* > 0$. In the region $\sigma_{ind}^* < 0$, in contrast, $|\Delta z_c|$ becomes larger than 0.04 Å and keeps increasing towards the limit of electron leakage.

Figures 6(a)–6(c) show the computed full-half-width, λ, for Li, Al, and Ag as a function of σ_{ind}^*, again computed with the PC method. Values increase as σ_{ind}^* decreases, in qualitative agreement again with previous results results for jellium [17]. We find $\Delta\lambda$ values are always lower then 0.01, 0.013, and 0.02 Å for Li, Al, and Ag, respectively, for the whole range of σ_{ind}^*, even in the vicinity to electron leakage. We observe only one point for the Ag(110) which gives a difference of 0.03 Å for $\sigma_{ind}^* = -6.63 \times 10^{-3}$ e/Å^2, which is probably due to a numerical error. Even so, these differences are smaller than those found for the $z_c - z_J$ values. We then conclude that the main reason for the discrepancies between method E_z and method PC come from the computation of the $z_c - z_J$ for large negative values of σ_{ind}^*. Nevertheless, for the rest of the σ_{ind}^* domain, we conclude that the electrostatic response for methods E_z and PC is equivalent. To our knowledge, this is the first numerical demonstration for this equivalence beyond linear response.

To validate these results, we have compared with previous DFT work using explicit slabs and jellium. It appears that not all the slab models computed in this work have been previously addressed with DFT. To our surprise, the profiles for Li(110), Li(111), Al(100), Ag(100), and Ag(110) of Figs. 6(a)–6(c) might be the first ever reported results beyond linear response using DFT for finite slabs and PPs. For all the other surfaces considered in previous work, we find a good level of agreement in general and the reader is referred to sec. VIII of Ref. [53] for a more detailed discussion.

Previous DFT work for Al(110) and Al(110) slabs only focused on positive values of σ_{ind}^*, and computed external fields as large as 5.0 V/Å [12]. Positive fields induce positive values for σ_{ind}^*. Such magnitudes for the external field could be well computed with the method PC, as the problem of electron leakage is not manifested. However, the main scope of the present work is to compare the electrostatic response between methods E_z and PC. In fact, if we applied fields
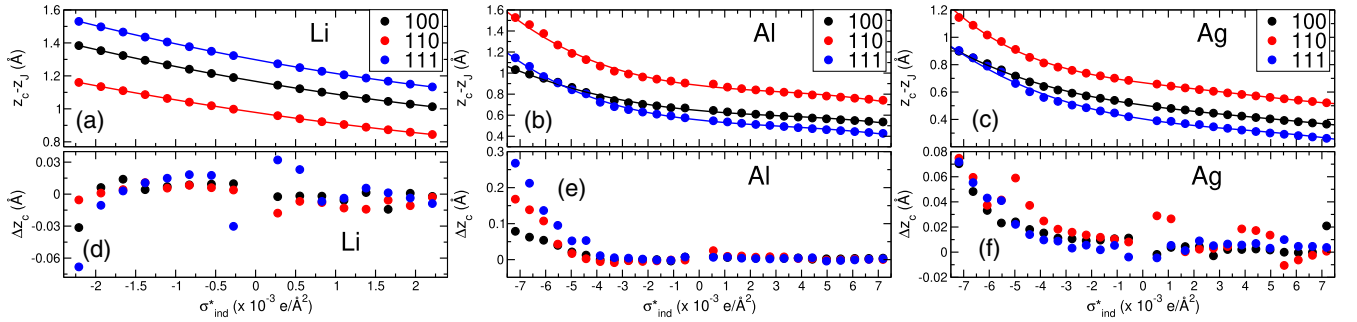
FIG. 5. [(a)–(c)] Values of $z_c - z_J$ as a function of the induced charge at the slab σ^*_{ind} computed the method *PC*. [(d)–(f)] Differences in z_c (Δz_c) between method E_z and method *PC*. Values are compared for the three facets for Li, Al, and Ag. Trend lines correspond to fourth-order polynomial fits to estimate values of $z_c - z_J$ for $\sigma^*_{ind} = 0$.

larger than 1.6 V/Å to neutral Al slabs, for example, the complementary response at the opposite side of the slab will be the accumulation of negative charge which will eventually lead to electron leakage.

The computation of vacuum-exposed surfaces under strong electric fields has historically aimed to evaluate the response of electrode surfaces in electrolytic cells, for example. We argue that for vacuum-exposed surfaces, a field that accumulates positive charge will only manifest in reality if there is a counter metallic surface negatively charged. However, beyond a certain value for the external field, electrons at the negative surface will start leaking toward the positive surface driven by the electrostatic force, and the assumption of a isolated surface would be not longer valid. Thus the largest realistic field will be subject to the lowest value of σ^*_{ind} at counter electrode before electron leakage starts to manifest.

Table I shows the computed response parameters $z_{c0} - z_J$ and λ_0, in the limit of $\sigma^*_{ind} = 0$ for all the slab models. These values are computed from interpolation of the computed data of Figs. 5 and 6, obtained using the method *PC*. Results are in good agreement with previous work and we refer the interesting reader to Sec. VIII B of Ref. [53] for further details.

In Table I, we also report the absolute difference $|\Delta z_{c0}|$ and $|\Delta \lambda_0|$ with respect to $z_{c0} - z_J$ and λ_0 computed with the method E_z, again via interpolation. The largest difference $|\Delta z_{c0}|$ between both methods is computed for the Ag(110) surface (2.6%). For $|\Delta \lambda_0|$, the largest difference is obtained for the Ag(100) surface (1.3%). Such deviations are within the expected numerical accuracy, and we can confidently claim

that methods E_z and *PC* are equivalent in the linear response regime. As far as we are concerned, the results of Table I provide the first numerical demonstration of the LK equivalence for finite slabs in PBCs using the PPs approximation. In contrast to the semi-infinite jellium model, the theoretical demonstration of such equivalence for finite jellium slabs is not trivial in principle but it deserves consideration of future research.

Localized basis sets can be used to control electron leakage in DFT simulations. However, for large negative values of σ^*_{ind}, this approach constrains the polarization of the surface electrons, which could potential lead to an unphysical description of the problem. For plane waves, such a constrain is subject to the distance between the dipole plane and the surface layer.

Prompted the work of Nguyen *et al.* [87] and I. Sarria *et al.* [88], a follow up direction of the present study could be the study of the dependence of z_{c0} on the crystallographic orientation (as considered here) and the thickness of the modelled slabs. The oscillations observed in the surface energy and work function for Al films as a function of film thickness [87] are attributed to the energies of confined electrons relative to the Fermi level and can be well fitted by a damped sinusoidal function, with the periodicity determined by the combination of either one or three Fermi wave vectors, depending on the facet under consideration. Corroborating such findings for z_{c0} would therefore be of fundamental relevance to investigate the interplay between the electrostatic response and quantum size effects.
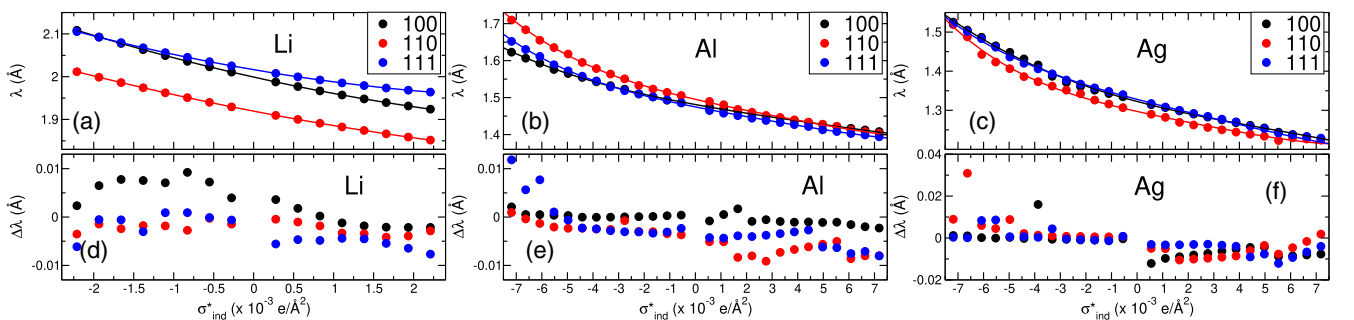

FIG. 6. [(a)–(c)] Values of λ as a function of the induced charge at the slab σ^*_{ind} computed the method *PC*. [(d)–(f)] Differences in λ ($\Delta\lambda$) between method E_z and method *PC*. Values are compared for the three facets for Li, Al, and Ag. Trend lines correspond to fourth-order polynomial fits to estimate values of λ for $\sigma^*_{ind} = 0$.
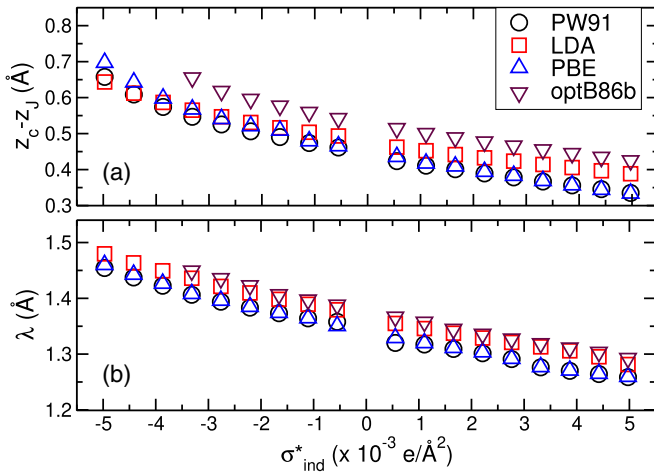
FIG. 7. Computed values for $z_c - z_J$ (a) and λ (b) as function of the total induced charge, σ^*_{ind}, for the Ag(111) slab using different XC functionals. Results were computed with the method *PC*.

VII. DEPENDENCE ON THE XC

In this section we investigate how the response parameters depend on the XC functional. To this purpose, we have considered the Ag(111) slab model. Based on the demonstrated equivalence of the previous sections, we have only computed the DFT problem with the *PC* method.

Results for $z_c - z_J$ in Fig. 7(a) show that PBE and PW91 (GGA-PW91) perform practically the same over the whole range of σ^*_{ind} as expected, being both XC functionals of GGA-type. Small differences only manifest for σ^*_{ind} values in the vicinity of electron leakage. LDA values agrees well with both PBE and PW91 for $\sigma^*_{\mathrm{ind}} < 0$, but the slope slightly depart for $\sigma^*_{\mathrm{ind}} > 0$. On the other hand, vdw-optB86b results in noticeable differences. First, differences in $z_c - z_J$ are as large as 0.1 Å with respect to the other functionals over the whole range of σ^*_{ind}. Second, and probably more relevant to the present study, we observe electron leakage for values below -3.31×10^{-3} e/Å², which are larger than for the other XC approximations. This demonstrates that the electrostatic response of negatively charged slabs can be significantly affected when including nonlocal corrections. This finding should be taken into account to revise the extend of physically valid σ^*_{ind} for vacuum-exposed metallic slabs. Finally, results of 7b for λ confirm that PBE and PW91 functionals are equivalent to describe the electrostatic response. Surprisingly, LDA and optB86b give practically the same values over the whole range of common σ^*_{ind}.

To evaluate the performance of the XC functionals, it would be required to perform a high-level benchmark simulation beyond DFT, such as RPA or *GW*. For the jellium model, several high-level calculations were performed over the years [89]. For a bare metallic slab using PBCs and the PP method, in contrast, we are only aware of the work of I. D. White *et al.* [45], who applied the *GW* space-time method to a Al(111) slab, and calculated the effective local potential experienced by electrons in the near-surface region. From the fitting of the potential in the vacuum region, I. D. White *et al.*

determined that the position of the image plane, z_{im}, is much closer to the outermost atomic layer than z_{c0}, which is the value of z_c extrapolated to the linear response regime. Note that the values of z_c are computed from purely electrostatic perturbations, whereas z_{im} is the result of a *GW* simulation of an unperturbed, neutral slab.

To our understanding, however, the prospect to applying a high-level method beyond DFT to compute (i) a neutral slab in an external field or (ii) a charged slab interacting with a perfect conductor, so that one could obtain z_c as a function of σ^*_{ind} [as in Fig. 7(a)], is beyond the reach of methods and related software implementations currently available. Apart from the well-known technical difficulties to converge any high-level method beyond DFT, particularly for metallic systems [90], we are not aware of any available RPA or *GW*-like method that can efficiently compute the quantum problem of an explicit slab (i.e., not jellium) under external perturbations. Future efforts along this line of research will indeed be beneficial to extend the scientific reach of the DFT and beyond-DFT communities.

VIII. CONCLUSIONS

In this work, we carried out detailed DFT simulations of vacuum-exposed metallic slabs under external fields. Using plane waves and PPs we computed the electrostatics for the (100), (110), and (111) facets of Li, Al, and Ag in PBCs. We compared the electrostatics response of neutral slabs in uniform electric fields with the response of charged slabs interacting with a PC located in the vacuum region. To this purpose, we analyzed profiles for induced potentials and charges and evaluated the role of slab thickness. To quantify how the electrostatic response depends on the strength of the external perturbation, we used two response parameters: the centroid of the induced surface charge, z_c, and its full-half-width, λ. Results demonstrate the numerical equivalence between the response of neutral and charged slabs for hole accumulation. The equivalence for electron accumulation also holds as long as the system response remains "far" from the condition of electron leakage. Surprisingly, there is no evidence of previous work for Li(110), Li(111), Al(100), Ag(100), and Ag(110), and our results appear to be the first ever reported DFT results for these surfaces beyond linear response using finite slabs in PBCs.

Analysis of this equivalence for Li slabs of different thicknesses show that only few layers are enough to capture most of the surface effects of metallic systems, but the number depends on the facet under consideration. The computed values of z_c and λ demonstrate a qualitative different behavior for electron and hole accumulation, in agreement with previous work. Interpolation of computed values allows accessing the limit of linear response and validate the KL equivalence. To the best of our knowledge, our work provides the first numerical demonstration of the LK equivalence using finite slabs in PBCs. The theoretical demonstration of such equivalence for finite jellium slabs is still a pending task in the field, for which it deserves the consideration of future work.

We also evaluated the dependence of the XC and found that the vdW-corrected optB86b functional leads to electron leakage for less negative surface densities in comparison with

standard LDA and GGA functionals. It is of further interest to carry out a similar analysis for other materials and corroborate the findings of this work.

The use of localized basis sets, instead of plane waves, offers a robust solution to control electron leakage from metallic surfaces when using external fields applied to neutral slabs. Nevertheless, depending on the value of the induced $\sigma_{\mathrm{ind}}^* = -e/A$ and the location of the dipole plane, unphysical solutions can be computed, as the charge would rather leak from the metallic surface driven by the electrostatic force. For this reason, we believe that future DFT studies with localized basis sets should consider carefully the case of electron accumulation.

In semiclassical models, the aim is to remove the explicit metallic slabs and approximate its electrostatic response using a PC located at the image plane position $z_{\mathrm{im}} = z_{c0}$. This setting implicitly assumes the linear response regime. The situation is different for systems of finite area in PBCs. In fact, electron transfer to unbound atoms/molecules will induce a nonzero

value of $\sigma_{\mathrm{ind}}^* = -e/A$ at the metallic slabs and a charge distribution with a centroid $z_c \neq z_{c0}$. Consequently, if one aims to approximate the response of a metallic surface in PBCs, setting the position of the PC plane at z_{c0} is incorrect.

Besides validating and extending previous work in the fundamentals of DFT simulations of metals, the present findings consolidate the basis for future extension of semiclassical DFT-based methods, for example towards TD-DFT and associated frequency-dependent electrostatic responses.

ACKNOWLEDGMENTS

[1] W. Kohn and L. J. Sham, Phys. Rev. **140**, A1133 (1965).
[2] P. Hohenberg and W. Kohn, Phys. Rev. **136**, B864 (1964).
[3] N. D. Lang and W. Kohn, Phys. Rev. B **1**, 4555 (1970).
[4] N. D. Lang and W. Kohn, Phys. Rev. B **3**, 1215 (1971).
[5] N. D. Lang and W. Kohn, Phys. Rev. B **7**, 3541 (1973).
[6] J. K. Nørskov, F. Abild-Pedersen, F. Studt, and T. Bligaard, Proc. Natl. Acad. Sci. **108**, 937 (2011).
[7] A. Michaelides and M. Scheffler, An introduction to the theory of crystalline elemental solids and their surfaces, in *Surface and Interface Science: Concepts and Methods*, edited by Klaus Wandelt (John Wiley & Sons Ltd., New Jersey, 2013), Chap. 2, pp. 13–72.
[8] A. Groß, *Theoretical Surface Science: A Microscopic Perspective* (Springer-Verlag, Berlin, Heidelberg, 2013).
[9] M. W. Finnis, Surf. Sci. **241**, 61 (1991).
[10] M. W. Finnis, R. Kaschner, C. Kruse, J. Furthmuller, and M. Scheffler, J. Phys.: Condens. Matter **7**, 2001 (1995).
[11] S. Lam and R. Needs, Surf. Sci. **277**, 173 (1992).
[12] S. C. Lam and R. J. Needs, J. Phys.: Condens. Matter **5**, 2101 (1993).
[13] J. E. Inglesfield and G. A. Benesh, Phys. Rev. B **37**, 6682 (1988).
[14] G. C. Aers and J. E. Inglesfield, Surf. Sci. **217**, 367 (1989).
[15] J. E. Inglesfield, Philos. Trans. R. Soc. Lond. A **334**, 527 (1991).
[16] W. Schmickler and D. Henderson, Phys. Rev. B **30**, 3081 (1984).
[17] P. Gies and R. R. Gerhardts, Phys. Rev. B **33**, 982 (1986).
[18] F. Schreier and F. Rebentrost, J. Phys. C **20**, 2609 (1987).
[19] A. Liebsch, Phys. Scr. **35**, 354 (1987).
[20] M. Weber and A. Liebsch, Phys. Rev. B **35**, 7411 (1987).
[21] E. Leiva and W. Schmickler, Electrochim. Acta **39**, 1015 (1994).
[22] P. A. Serena, J. M. Soler, and N. Garcia, Europhys. Lett. **8**, 185 (1989).
[23] A. Kiejna, Phys. Rev. B **47**, 7361 (1993).
[24] A. Andriotis, Comput. Mater. Sci. **4**, 93 (1995).
[25] J. Neugebauer and M. Scheffler, Phys. Rev. B **46**, 16067 (1992).

[26] K.-M. Ho, B. N. Harmon, and S. H. Liu, Phys. Rev. Lett. **44**, 1531 (1980).
[27] C. L. Fu and K. M. Ho, Phys. Rev. Lett. **63**, 1617 (1989).
[28] C. G. Sńchez, A. Y. Lozovoi, and A. Alavi, Mol. Phys. **102**, 1045 (2004).
[29] C. G. Sánchez, E. Santos, and W. Schmickler, Phys. Rev. B **71**, 073404 (2005).
[30] A. Y. Lozovoi, A. Alavi, J. Kohanoff, and R. M. Lynden-Bell, J. Chem. Phys. **115**, 1661 (2001).
[31] A. Y. Lozovoi and A. Alavi, Phys. Rev. B **68**, 245416 (2003).
[32] A. Michl, J. Weissmüller, and S. Müller, Langmuir **34**, 4920 (2018).
[33] R. Jinnouchi, K. Kodama, and Y. Morimoto, Curr. Opin. Electrochem. **8**, 103 (2018).
[34] J. Jung, J. E. Alvarellos, E. Chacón, and P. García-González, J. Phys.: Condens. Matter **19**, 266008 (2007).
[35] J. P. Perdew and A. Zunger, Phys. Rev. B **23**, 5048 (1981).
[36] J. Klimeš, D. R. Bowler, and A. Michaelides, Phys. Rev. B **83**, 195131 (2011).
[37] K. Berland, V. R. Cooper, K. Lee, E. Schröder, T. Thonhauser, P. Hyldgaard, and B. I. Lundqvist, Rep. Prog. Phys. **78**, 066501 (2015).
[38] G. Binnig, N. Garcia, H. Rohrer, J. M. Soler, and F. Flores, Phys. Rev. B **30**, 4816 (1984).
[39] P. M. Echenique, J. M. Pitarke, E. V. Chulkov, and A. Rubio, Chem. Phys. **251**, 1 (2000).
[40] P. Garcia-Gonzalez and R. Godby, Comput. Phys. Commun. **137**, 108 (2001).
[41] L. A. Constantin, E. Fabiano, J. M. Pitarke, and F. Della Sala, Phys. Rev. B **93**, 115127 (2016).
[42] B. Kaduk, T. Kowalczyk, and T. Van Voorhis, Chem. Rev. **112**, 321 (2012).
[43] A. M. Souza, I. Rungger, C. D. Pemmaraju, U. Schwingenschloegl, and S. Sanvito, Phys. Rev. B **88**, 165112 (2013).
[44] D. D. O'Regan and G. Teobaldi, Phys. Rev. B **94**, 035159 (2016).

[45] I. D. White, R. W. Godby, M. M. Rieger, and R. J. Needs, Phys. Rev. Lett. **80**, 4265 (1998).

[46] I. Scivetti and M. Persson, J. Phys.: Condens. Matter **25**, 355006 (2013).

[47] I. Scivetti and M. Persson, J. Phys.: Condens. Matter **26**, 135003 (2014).

[48] I. Scivetti and M. Persson, J. Phys.: Condens. Matter **29**, 355002 (2017).

[49] S. Fatayer, B. Schuler, W. Steurer, I. Scivetti, J. Repp, L. Gross, M. Persson, and G. Meyer, Nat. Nanotechnol. **13**, 376 (2018).

[50] M. L. Perrin, C. J. O. Verzijl, C. A. Martin, A. J. Shaikh, R. Eelkema, J. H. van Esch, J. M. van Ruitenbeek, J. M. Thijssen, H. S. J. van der Zant, and D. Dulic, Nat. Nanotechnol. **8**, 282 (2013).

[51] C. J. O. Verzijl, J. A. Celis Gil, M. L. Perrin, D. Dulić, H. S. J. van der Zant, and J. M. Thijssen, J. Chem. Phys. **143**, 174106 (2015).

[52] N. Armbrust, J. Güdde, and U. Höfer, New J. Phys. **17**, 103043 (2015).

[53] See Supplemental Material at http://link.aps.org/supplemental/10.1103/PhysRevB.108.165423 for DFT formalism for metallic slabs in periodic boundary conditions; DFT formulation of a neutral slab in uniform electric field; the DFT-PC method; slab models and DFT settings; symmetry restrictions in DFT codes; induced potential and charge for the (110) and (111) facets; dependence on the slab thickness; and comparing the electrostatic response with previous work.

[54] E. V. Chulkov, V. M. Silkin, and P. M. Echenique, Surf. Sci. **391**, L1217 (1997).

[55] A. G. Eguiluz, M. Heinrichsmeier, A. Fleszar, and W. Hanke, Phys. Rev. Lett. **68**, 1359 (1992).

[56] E. V. Chulkov, V. M. Silkin, and P. M. Echenique, Surf. Sci. **437**, 330 (1999).

[57] M. Nekovee and J. M. Pitarke, Comput. Phys. Commun. **137**, 123 (2001).

[58] S. S. Tsirkin, A. G. Borisov, and E. V. Chulkov, Phys. Rev. B **88**, 035449 (2013).

[59] P. A. Serena, J. M. Soler, and N. García, Phys. Rev. B **34**, 6767 (1986).

[60] A. Hanuschkin, D. Wortmann, and S. Blügel, Phys. Rev. B **76**, 165417 (2007).

[61] N. Garcia, B. Reihl, K. H. Frank, and A. R. Williams, Phys. Rev. Lett. **54**, 591 (1985).

[62] J. W. Gadzuk, Surf. Sci. **23**, 58 (1970).

[63] J. Heinrichs, Phys. Rev. B **8**, 1346 (1973).

[64] V. M. Silkin, A. K. Kazansky, E. V. Chulkov, and P. M. Echenique, J. Phys.: Condens. Matter **22**, 304013 (2010).

[65] A. M. Gabovich and A. I. Voitenko, Eur. J. Phys. **33**, 1289 (2012).

[66] L. Bengtsson, Phys. Rev. B **59**, 12301 (1999).

[67] N. Luque and W. Schmickler, Electrochim. Acta **71**, 82 (2012).

[68] J. D. Jackson, *Classical Electrodynamics*, 3rd ed. (Wiley, New York, NY, 1999).

[69] K. Kempa, Surf. Sci. Lett. **157**, L323 (1985).

[70] F. Chao, Surf. Sci. **157**, L328 (1985).

[71] A. J. Cohen, P. Mori-Sánchez, and W. Yang, Science **321**, 792 (2008).

[72] P. J. Feibelman, Phys. Rev. B **64**, 125403 (2001).

[73] P. E. Blöchl, Phys. Rev. B **50**, 17953 (1994).

[74] G. Kresse and J. Furthmüller, Comput. Mater. Sci. **6**, 15 (1996).

[75] G. Kresse and J. Furthmüller, Phys. Rev. B **54**, 11169 (1996).

[76] G. Kresse and D. Joubert, Phys. Rev. B **59**, 1758 (1999).

[77] Y. Wang and J. P. Perdew, Phys. Rev. B **44**, 13298 (1991).

[78] D. M. Ceperley and B. J. Alder, Phys. Rev. Lett. **45**, 566 (1980).

[79] J. P. Perdew, K. Burke, and M. Ernzerhof, Phys. Rev. Lett. **77**, 3865 (1996).

[80] M. Methfessel and A. T. Paxton, Phys. Rev. B **40**, 3616 (1989).

[81] J. Junquera, M. H. Cohen, and K. M. Rabe, J. Phys.: Condens. Matter **19**, 213203 (2007).

[82] R. H. Fowler and L. W. Nordheim, Proc. R. Soc. Lond. A **119**, 173 (1923).

[83] E. L. Murphy and R. H. Good, Phys. Rev. **102**, 1464 (1956).

[84] Y. Gohda, Y. Nakamura, K. Watanabe, and S. Watanabe, Phys. Rev. Lett. **85**, 1750 (2000).

[85] B. Lepetit, J. Appl. Phys. **122**, 215105 (2017).

[86] W. Harrison, *Solid State Theory*, Dover Books on Physics (Dover Publications, New York, 1980).

[87] D.-L. Nguyen, C.-M. Wei, and M.-Y. Chou, Phys. Rev. B **99**, 205401 (2019).

[88] I. Sarria, C. Henriques, C. Fiolhais, and J. M. Pitarke, Phys. Rev. B **62**, 1699 (2000).

[89] J. M. Pitarke, L. A. Constantin, and J. P. Perdew, Phys. Rev. B **74**, 045121 (2006).

[90] T. Olsen and K. S. Thygesen, Phys. Rev. B **87**, 075111 (2013).